Thermal analysis of the debinding process of filaments with H13 steel powder

Michał Gocki[1*], Grzegorz Matula[1] (ID)

[1] Scientific and Teaching Laboratory of Nanotechnology and Material Technologies, The Silesian University of Technology, Towarowa 7a, Gliwice, Poland
* Corresponding author's e-mail: michal.gocki@polsl.pl

ABSTRACT

The FDM method, which employs a metal powder filament with a polymer binder, results in the production of sintered H13 steel. The technique is characterised by a multi-step process, low cost, and no waste, rendering it suitable for both small and medium-scale production. Nevertheless, the successful production of H13 steel parts using this method hinges on the meticulous design of the process to eliminate the polymeric binder that serves as an elastic matrix for the metal powder in the filaments. A study was conducted to identify the optimal conditions for binder debinding and powder sintering, and to evaluate their efficacy in relation to the type of filaments comprising a significant proportion of H13 steel powder. Furthermore, the chemical structure of the polymers was analysed by FTIR spectroscopy, with consideration given to the impact of varying debinding parameters. Furthermore, the morphology and structure of the material following the printing and sintering processes were investigated using scanning electron microscopy. Thermal analysis plays a pivotal role in the design of novel material fabrication techniques utilising Metal FDM technology. It allows for the comprehension of the thermal properties of materials, thereby facilitating the optimisation of process conditions. The findings of the study present an alternative approach to the manufacturing of metal components through sintering, and emphasise the significance of optimisation processes.

Keywords: thermal analysis, 3D printing, MFDM technology, H13 steel.

INTRODUCTION

The high costs of machinery and production have contributed to the limited adoption of single-step additive metalworking processes in small companies and laboratories [1]. In light of economic considerations, multi-step processes that produce composite parts by layering, whereby the requisite properties of the finished parts are achieved through binder removal and sintering processes, are gaining popularity. The most prevalent manufacturing techniques, collectively termed 'multistage', encompass MFDM (metal fused deposition modelling) and PIM/MIM (powder/metal injection molding) [2, 3]. These methods offer several advantages, including the absence of an expensive heat source during printing (such as a laser, electron beam, or electric arc) and the absence of a controlled atmosphere

during printing. The FDM printing of H13 steel is based on the extrusion of a plastic material through the extruder head, which is then applied layer by layer using an additive method to the printer's work table. Subsequently, additional processing is required for the part produced in this way. This consists of binder removal, which encompasses chemical and thermal debinding, as well as a sintering process.

Advanced research on 3D printing focuses on many variables that have a direct impact on the quality and strength of printed elements. Among the key studies conducted by scientists is the investigation of the effect of layer height and wall thickness on the mechanical strength of the print. The thinner the layers and the thicker the walls, the more uniform the structure, which increases resistance to mechanical loads [4]. Another important aspect is post-print surface treatment,

which improves surface smoothness and eliminates defects, crucial in applications requiring high precision. This issue is addressed in studies carried out at the Technical University of Baghdad [5], and the problem of roughness after the metallization process of samples produced by 3D printing was addressed in these studies [6]. Additionally, the influence of infill density on the strength of the model is well known [7].

In more advanced printing technologies, such as metallic FDM (fused deposition modeling), post-processing issues become even more complex and require precise optimization at the material level. It is crucial to select the appropriate thermal degradation temperature of the polymer binder used in the filament, as well as the sintering parameters of the metal powder [8, 9]. Improper settings of these parameters can lead to incorrect microstructure, which in turn affects the final mechanical properties and strength of the produced metal components.

The article describes the process of selecting binder removal and sintering conditions for filaments filled with H13 steel powder. The chemical structure of the binder polymers, as well as the morphology and structure of the material after printing and sintering were also investigated. The results described provide insights into key processes for optimising the production of metal parts by MFDM. The thermal decomposition analysis of the polymers contained in the filament binder also plays an important role in this article. For this reason, the authors introduce readers to the physicochemistry of polymers.

In the thermal removal of polymeric material, the dissociation energy of the weakest bonds of the polymer molecule plays a key role [10]. The physical and chemical properties of polymers, including their stability under thermal conditions, are closely related to the dissociation energy, affecting the durability and behaviour of these materials in different environments [11].

Fundamental to this is the role of dissociation energy in relation to a polymer's resistance to binder removal processes. Polymer structures consist of long chains of molecules linked by different types of bonds, such as covalent bonds, hydrogen bonds or Van der Waals forces. Among these, there are weaker bonds, which are more susceptible to breaking under certain conditions, such as exposure to solvents or elevated temperatures.

Thermal bond removal involves the gradual decomposition of the polymer structure when exposed to temperature. The heat energy supplied raises the kinetic energy of the polymer molecules, which can lead to the fracture of the least durable bonds. If the dissociation energy of these bonds is low, the polymer becomes more susceptible to thermal degradation. Conversely, in polymers with higher dissociation energies, the bond removal process may occur more slowly or require higher temperatures [12].

A theory proposed by Dutch chemist van der Krevelen refers to the relationship between the dissociation energy of the most sensitive bond in a molecule and the half-life temperature ($T_{1/2}$), which represents the temperature at which half of the substance decomposes. According to this theory, there is a direct correlation between the dissociation energy, the energy required to break a given bond, and the half-life temperature of a substance [13, 14].

Sintering is a fundamental metallurgical process that transforms loose metallic powder particles into a cohesive and solid material. The process operates at temperatures below the melting point of the metal or alloy, typically between 60–80% of the melting point, allowing for atomic diffusion without actual melting [15–17]. As sintering progresses, the metal powder particles form necks, form necks at points of contact, which leads to displacement and compaction. This displacement increases the packing of the particles, increasing the overall density of the sinter. Sintering is a complex process that involves atomic diffusion, where atoms migrate to minimize surface energy, spheroidization of pores, and their subsequent elimination. Precise control over temperature and sintering time is essential to achieve the desired level of densification. In addition, a reducing atmosphere is used to prevent oxidation of the sample surface layer [15].

The aim of the research was to determine the optimal conditions for polymer binder removal and the sintering process in 3D printing technology using the FDM method with a filament containing H13 steel powder. This process is crucial for achieving high-quality final metal components, as effective polymer binder removal is essential to ensure the proper structure and mechanical properties of the sintered parts. The study focused on analysing the debinding parameters, which have a significant impact on the sintering process and the final properties of the H13 steel components.

MATERIALS

The subject of this work is two filaments based on H13 steel powder with high fill density. The first material is a commercially available Zetamix H13 filament, while the second is an experimental filament produced at the Silesian University of Technology. Both filaments are designed for use in Metal Fused Deposition Modelling (Metal FDM) technology [18].

The Zetamix H13 filament is made from high-grade H13 steel powder; the finished sinters made from this material provide excellent durability and resistance to high temperatures. H13 steel is particularly suitable for industrial applications such as hot work tools and injection moulds. The filament exhibits exceptional mechanical properties, enabling the precise printing of parts with complex shapes [16, 19]. Unfortunately, the manufacturer does not specify the binder composition of the filament. In commercially available steel powder filaments, particle sizes range from 3 to 40 μm [20]. According to the manufacturer's specifications, the volume ratio of powder to binder in the commercial filament is 52% [21].

The binder in the experimental filament was made from a blend of high-density polyethylene (HDPE), acrylonitrile-butadiene-styrene terpolymer (ABS) and ethylene-vinyl acetate copolymer (EVA). The volume ratio of the blend consisted of 45% steel powder, 20% EVA, 20% ABS, and 15% HDPE. This combination of polymers results in a relatively low binder viscosity and allows the use of a solvent (in the form of acetone) in one of the binder removal steps. The H13 steel powder used

to make the author's filament had particle sizes ranging from 1 to 38 μm.

To produce the metal-filled filament, the steel powder was mixed with a multi-component polymer binder using a Zamak Mercator kneader at a screw speed of 40 rpm at 170 °C. From this prepared mixture, the filament was extruded to a diameter of 2.85 mm using a ZAMAK MERCATOR laboratory conical twin-screw extruder with a screw speed of 60 rpm.

The extrusion temperature of the material in the individual zones ranged from 160 to 175 °C. At the beginning of the screw, where the material enters the extruder, the temperature was the lowest at 160 °C, and then it gradually increased to reach 175 °C in the last zone. The process was carried out in an extruder equipped with a twin-screw system, with each screw having a length of 16.5 cm (L). Due to the conical design of the screws, their diameter ranges from 20 mm to 5 mm (D).

The particle size distribution of the H13 steel powder used for the experimental filament is shown in Figure 1. In addition, thermal debinding of the commercial filament was performed, and the remaining steel powder was crushed in a ceramic mortar to break up any agglomerates and is also shown in Figure 1 for comparison.

METHODS

The experimental filament and the Zetamix filament undergo different binder removal and sintering processes, differ due to the presence of
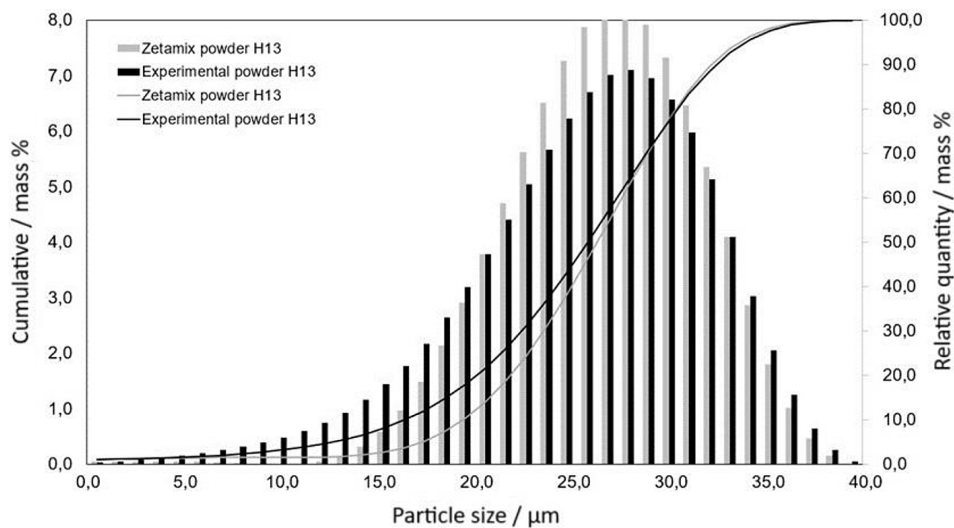

Figure 1. Particle size distribution of the powder

various polymer binder components in the two materials. The experimental filament contains an acetone-soluble polymer, while the Zetamix product does not contain this type of polymer and is only subjected to a thermal binder removal process at a maximum temperature of 480 °C [22]. At this temperature, the macromolecular structure of the binder fragments and disintegrates, leaving a pure powder [20]. Acetone is used as a solubilising agent in the Metal FDM process, effectively dissolving the ABS polymer in the newly developed filament. The dissolved ABS component in acetone can be recovered and reused as recyclate [23], which can be employed to produce new components, helping to reduce the waste generated in the Metal FDM process. The acetone recycling process starts with the separation of acetone from the dissolved ABS polymer. The acetone is then subjected to a distillation process, where it can be purified and recovered for further use. The purified acetone can be reused to degrade the printed parts, creating a closed-loop recycling system. This process reduces waste and minimises the consumption of raw materials by reusing the ABS polymer. Recycling acetone is a significant step towards a more sustainable approach to the production and use of materials in Metal FDM technology. This process reduces the environmental impact by reducing the waste generated during 3D printing [24]. The selected polymeric components in the experimental filament ensure that a relatively low viscosity binder is obtained and that the solvent, acetone, can be used in one of the binder debinding steps. The use of acetone as a solvent for one of the binder components allows pores to form throughout the material, which then facilitates the thermal debinding of the other binder components. The choice of acetone as a solvent was based on the solubility parameters of ABS and acetone, calculated using Van Krevelen's theory [13]. The other compounds used to make the experimental filament were EVA copolymer and HDPE. The EVA copolymer adds flexibility to the resulting filament, while high-density polyethylene serves as a backbone polymer to maintain the shape of the sample during the final stages of thermal binder removal. During the thermal removal of the binder without oxygen, the material pyrolyses to form gaseous products. The selection of polymer components for the blend was the result of extensive physico-chemical analyses based on the literature [13, 14]. The final result was a material with suitable properties.

During thermal debinding, the polymer binder breaks down. This process varies depending on the use of the specific polymers present in the binder. In the initial heating phase, the sample may release gases such as CO_2, CO, water vapor, and hydrocarbon compounds. In the second stage, selected functional groups may dissociate and form organic compounds, while in the final stage, the polymer chains are broken down by weakening the carbon-carbon bonds [10]. The thermal debinding process for both tested materials was conducted over a period of 42 hours. For the commercial material, two isothermal holds, each lasting 1 hour, were applied – the first at 355 °C and the second at 470 °C. In the case of the experimental material, the isothermal holds also lasted 1 hour but were set at higher temperatures: the first at 420 °C and the second, similarly to the commercial material, at 470 °C. The selection of isothermal holds was based on thermogravimetric analysis (TGA) results, which precisely identified the temperature ranges where the key stages of binder removal occurred. The process was carried out in a tubular furnace manufactured by Czylok.

After binder debinding, both filaments are sintered in a N_2-10%H_2 atmosphere at 1350 °C. The heating rate of the system during the sintering process was 200 °C/h, and the isothermal stop at 1350 °C lasted 30 minutes. During sintering, the pores between the powder particles are spheroidised and then annihilated, leading to an increase in sinter density and material shrinkage. In summary, the process of chemical and thermal removal of the binder from the laboratory filament is more complex due to the presence of the acetone-soluble polymer. The Zetamix filament undergoes only the thermal binder removal and sintering processes. Both sintering processes take place in an atmosphere of N_2-10%H_2 which is crucial to achieve the desired quality and properties of the metal product.

The research was conducted using a high-resolution scanning electron microscope (Zeiss Supra 35) at an accelerating voltage of 20–10 kV and magnifications of 500–5.000×. A secondary electron detector (SE) was used for the analysis.

Thermogravimetric analysis (TG) and derivative thermogravimetric analysis (DTG) are thermal analysis techniques that use the variation of a sample's mass as a function of temperature. A TG plot shows the mass of a sample as a function of temperature, while a DTG plot is the derivative of a TG thermogram and presents the rate of mass

change as a function of temperature. The peaks in the DTG plot are related to different stages of decomposition or other thermal processes in the material [25, 26]. The thermogravimetric analysis was performed using a Netzsch STA 409 PC/PG thermowell. The conditions for thermogravimetric (TG) analysis were as follows: the sample mass was 45 mg, and the heating rate was set at 10 °C/min. Measurements were conducted in an argon atmosphere to prevent sample oxidation, within a temperature range of 43 °C to 600 °C.

FTIR (Fourier transform infrared) analysis of polymeric materials is commonly used to study their chemical structure. FTIR studies were carried out using a Termo Scientific Nicolet 6700 spectrometer. Microscopic analysis was conducted using a high-resolution scanning electron microscope (HRSEM), the SUPRA 35 model, manufactured by Zeiss. The samples for FTIR analysis, after being removed from the furnace, were immediately placed in a desiccator where a constant temperature of 20 °C and normal humidity levels were maintained. This was done to minimize the impact of environmental factors, such as changes in humidity and temperature, on the samples before analysis. Prior to the FTIR examination, the samples were further ground in a ceramic mortar to achieve the appropriate particle size required for accurate FTIR analysis.

The FTIR measurement of the samples was performed using the ATR method (attenuated total reflectance). The measurement resolution was 4 cm^{-1}, and the spectral range covered from 2.5 μm to 25 μm, corresponding to the range of 4000 to 400 cm^{-1}.

RESULTS

Thermogravimetric analysis

Heating of the samples was carried out at 10 °C/min in an argon atmosphere. An atmosphere of inert gas acts as a protective layer, preventing oxidation on the surface of the powder particles. Consequently, the results of the thermogravimetric analysis allow for the measurement of the sample's weight loss as the temperature increases. This loss is related to the removal of the binder and reaches a minimum at 490 °C, followed by a gentle increase in mass. This increase is likely due to slight oxidation of the powder particle surfaces. The reason for this could be a lack of tightness in the measurement system or an oxygen-contaminated protective gas. Therefore, binder debinding of samples intended for further sintering should be performed in a reducing gas atmosphere rather than an inert gas.

The plot of the thermogravimetric curve (TGA) of the filament shown in Figure 2 provides important information on its thermal stability and debinding behaviour. The TG (thermogravimetric) curve shows that the polymer maintains a relatively stable mass from 43 °C to around 250 °C, indicating that there is no significant thermal debinding or loss of volatile compounds in this temperature range. Thereafter, A slight decrease in mass begins at approximately 250 °C, followed by a more pronounced decrease starting at around 315 °C and continuing until about 405 °C. This portion of the curve corresponds to the debinding of the first
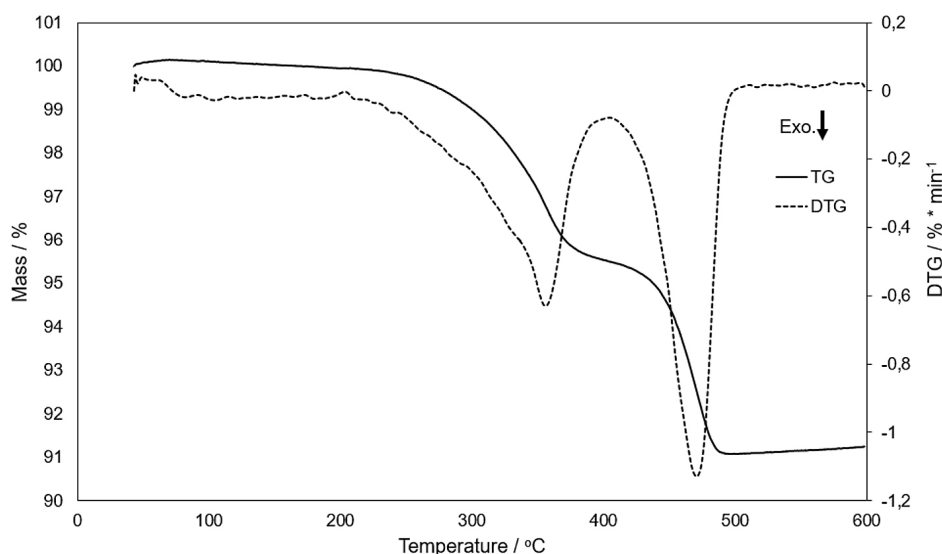

Figure 2. Results of thermogravimetric analysis of the Zetamix H13 filament. TG and DTG test

component of the filament. Above 405 °C, the rate of mass loss slows down and the curve stabilises to around 430 °C. Above this value, the mass of the sample starts to decrease again, a process that continues until 490 °C. In this range, debinding of the second polymer component has occurred. Beyond 490 °C, there is a slight increase in the mass of the test sample. From the TG, we can determine the value of the sample weight loss (Δm), which amounted to 9% for the whole process. An important element in the analysis is the consideration of the weight loss during the individual stages of material decomposition. In the first and second stages, the weight loss was approximately 4.5%. The remaining mass of the sample after thermogravimetric testing was 91%.

The DTG (thermogravimetric derivative) curve reveals two distinct peaks. The first peak occurs around 355 °C, at which the debinding of the first polymer is most intense – 0.63%/min. The second peak occurs around 470 °C and shows that the second polymer at this temperature shows the highest debinding rate - approximately 1.1 %/min. On this basis, and on the basis of other results such as FTIR, it can be concluded that the first polymer component was polyvinyl acetate and the second polyethylene (Figure 3).

The TG (thermogravimetric) curve shows that the polymer maintains a relatively stable mass from 43 °C to about 270 °C, indicating no significant thermal debinding or loss of volatile compounds in this temperature range. However, a more pronounced decrease in mass begins once 300 °C is reached and continues until about 400 °C. After 400 °C, the mass of the sample decreases rapidly, with the TG curve only stabilising around 495 °C. The value of the total weight loss of the sample was 13.5 per cent. In the first stage of the process from 43 °C to 400 °C, the mass loss value was 1.2 per cent, while in the second stage in the temperature range 400 °C to 500 °C, the sample lost 12.3 per cent of its mass. The remaining mass of the sample after thermogravimetric testing was 86.5%. This mass corresponds to a powder polymer of 13.5% (w/w).

Thermogravimetric derivative (DTG) analysis reveals two significant peaks in the maximum mass loss rate at different stages of the process. The first occurs at 420 °C and indicates the fastest mass loss of the first polymer component, at 1.03% per minute. The second peak occurred at 472 °C and the fastest weight loss rate of the second polymer was 2.15% per minute.

SEM analysis

SEM analysis allows a number of observations to be made about the structure of the filaments. In the case of the experimental filament, post-extrusion surface images (Fig. 4) confirm the presence of a powder fraction with a more diverse range of particle sizes compared to the Zetamix filament (Fig. 1). It should also be noted the higher polymer binder content on the surface of the experimental filament than in the commercial material. This difference is due to the higher metal powder content in the Zetamix filament. During the chemical debinding of the experimental
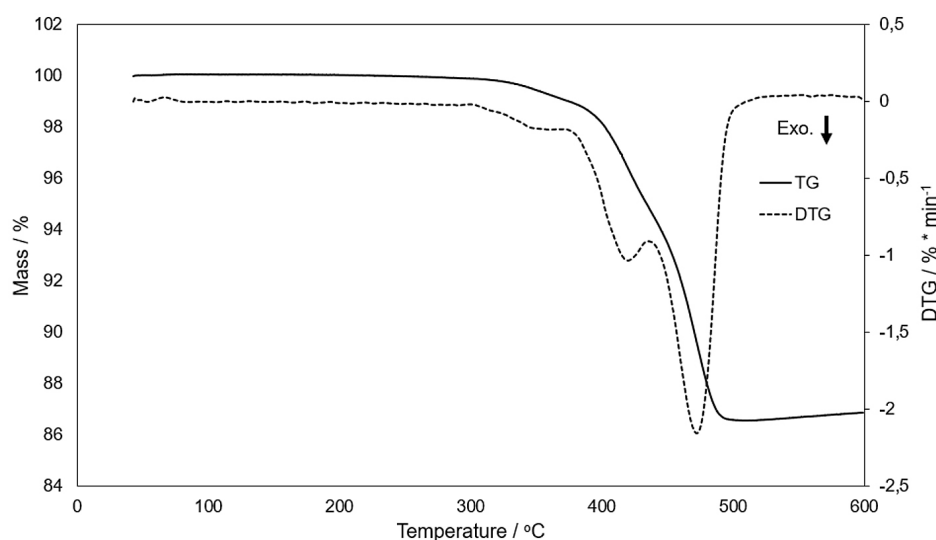

Figure 3. Results of thermogravimetric analysis of the experimental filament. TG and DTG tests

filament, a reduction in the amount of binder on the surface was observed, accompanied by the appearance of pores between 20 and 30 µm in size (Fig. 5). The surface of the experimental filament (Fig. 5a) shows the presence of an acetone-insoluble polymer (HDPE and EVA) on the surface layer of the filament.

After the thermal debinding process, the presence of powder particles on the surface of the filament intensifies. (Fig. 6). Analysis of Figures 6b and 6d suggests that both the experimental and commercial material used powders containing spherical particles; in addition, agglomerates of powder particles are present in the experimental filament.

According to the measurement of the fraction size with the particle size analyser (Fig. 1), the SEM images (Fig. 6) confirm the fact that the commercial felt has a larger number of particles in the 7–20 µm range. Furthermore, the experimental felt has a wider particle size distribution than the commercial material. Comparing the two scanning electron microscopy (SEM) images showing the

surface of the filaments after the sintering process, significant differences between the commercial and experimental filaments are clearly visible (Figs. 7a and 7b). There is a noticeably lower number of pores on the surface of the commercial filament compared to the experimental filament. It should also be noted the deformation of the surface layer of the experimental filament, which is not present in the commercial filament. This phenomenon may be due to the higher polymer binder content in the experimental material. The higher polymer content results in greater material shrinkage.

Debinding mechanism of experimental filament

The FTIR analysis of the material containing EVA, HDPE and ABS, shown in the accompanying graph (Fig. 8), provides valuable information about the structural changes occurring during thermal processing. The reference spectrum (sample at 25 °C) is characterised by clear absorption bands
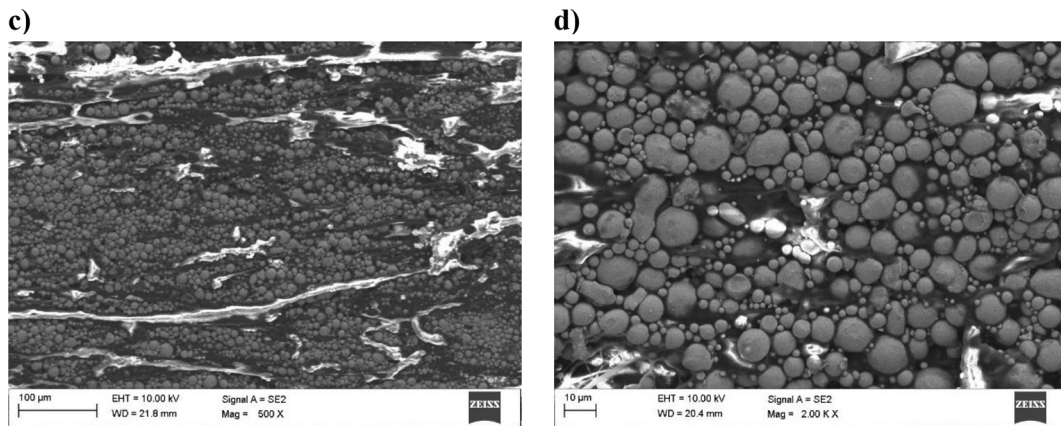

Figure 4. Surface morphology of the as-received Zetamix filament (a,b) and the experimental filament after extrusion (c,d)
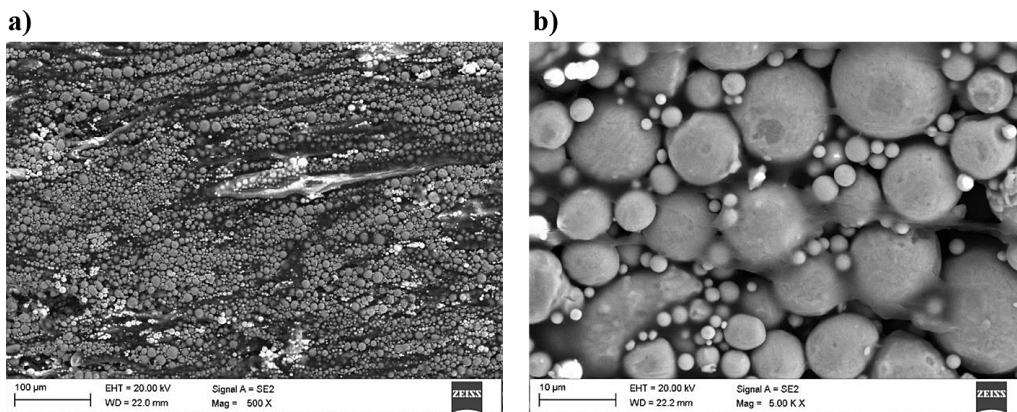

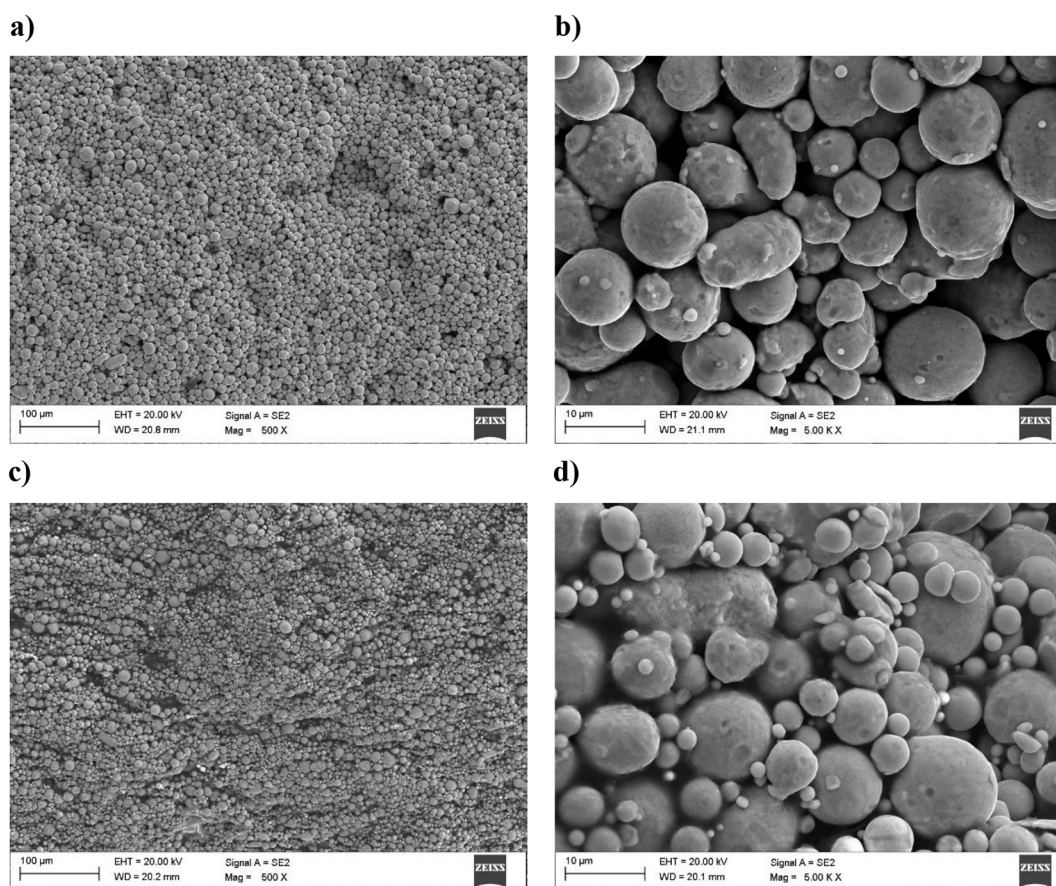**Figure 5.** Surface morphology of the experimental filament (a, b) after the chemical debinding

a)

b)

c)

d)

Figure 6. Surface morphology of the Zetamix filament (a,b) and the experimental filament (c, d) after the thermal debinding
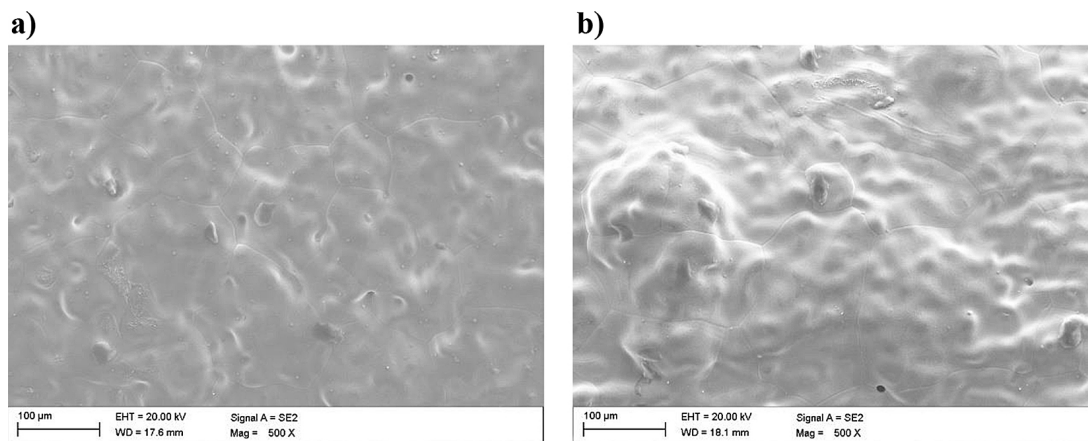
a)

b)

Figure 7. Surface morphology of the Zetamix filament (a) and the experimental filament (b) after the sintering

in the range 2900–2800 cm^{-1}, corresponding to C-H stretching associated with the methyl groups. Also visible are bands in the 1500–1400 cm^{-1} range associated with C-H deformations and a number of bands below 1000 cm^{-1}, which can be attributed to vibrations of the polymer backbone [26]. After thermal treatment at 350 °C (dashed curve), a significant reduction in the intensity of the absorption bands is observed, indicating thermal debinding of the polymer components. In particular, the reduction of bands in the 2900–2800 cm^{-1} and 1500–1400 cm^{-1} ranges suggests the breakdown of C-H groups, which is typical of EVA and HDPE debinding [27].
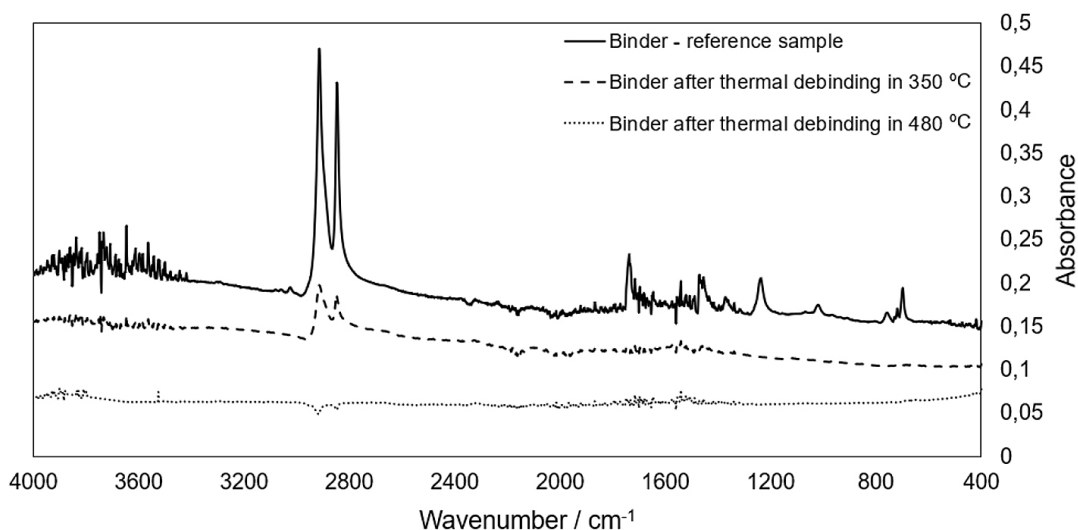
Figure 8. FTIR spectra of binder experimental filament

In the case of thermal treatment at 480 °C (dotted curve), a further reduction in the intensity of the absorption bands is apparent, with many of the characteristic bands virtually disappearing. This indicates a further, more advanced debinding of the polymers, leading to an almost complete breakdown of the material's parent structure. The disappearance of bands in the range below 1000 cm^{-1} suggests the breakdown of the polymer backbone, which is consistent with the high-temperature debinding of HDPE [28]. In summary, FTIR analysis shows that the material containing EVA, HDPE and ABS undergoes significant thermal debinding as early as 350 °C, and at 480 °C the polymer structure is almost completely decomposed.

Analysis of the qualitative composition of Zetamix filament

Examination of the FTIR spectrum for the Zetamix H13 filament revealed characteristic absorption bands that indicate the presence of polyethylene (PE) and polyvinyl acetate (PVAc). The FTIR spectrum is placed in Figure 9. The FTIR spectrum revealed distinct peaks in the 2800–3000 cm^{-1} range, which are typical of the C-H stretching vibrations in the methyl and methylene groups present in PE. In particular, strong peaks in the region of 2916 cm^{-1} and 2848 cm^{-1} are consistent with absorptions characteristic of aliphatic hydrocarbons. The presence of these bands confirms that polyethylene is an important component of the sample [26].
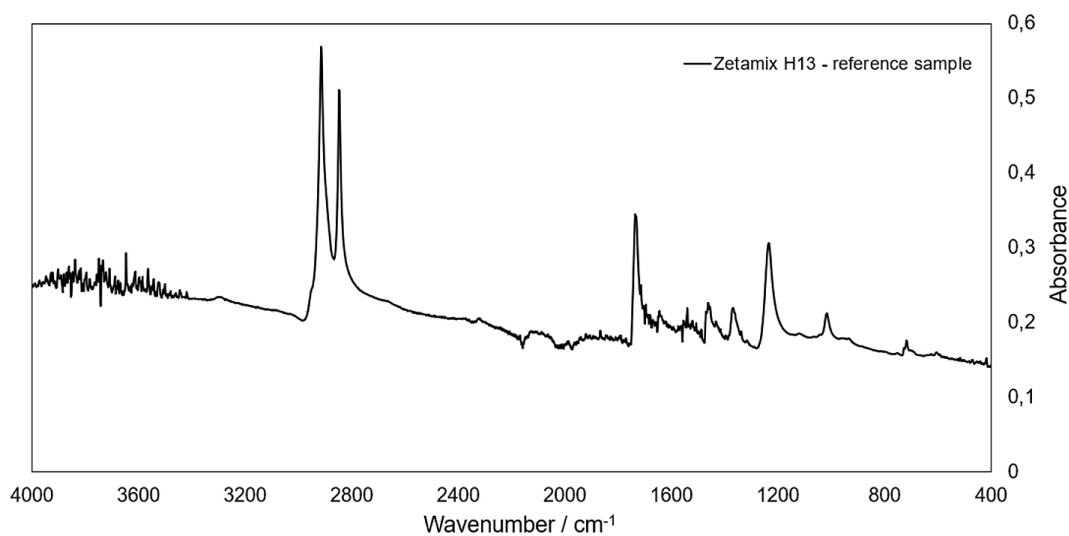

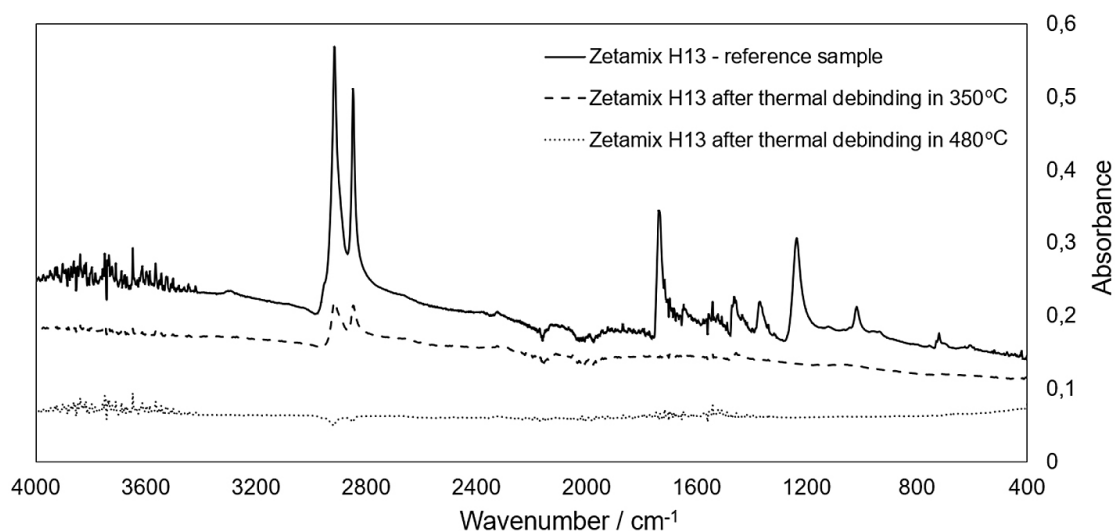**Figure 9.** FTIR spectra of Zetamix H13 filament

Figure 10. FTIR spectra of Zetamix H13 filament, reference sample and sample after thermal debinding

In addition, the FTIR spectrum revealed a band at 1735 cm^{-1}, characteristic of carbonyl groups (C = O) associated with acetate bonds in polyvinyl acetate (PVAc). This band is a key indicator of the presence of PVA, as the carbonyl groups are highly specific for this polymer. Furthermore, the absorption bands in the 1400–1500 cm^{-1} range correspond to C-H deformation vibrations, which are common to both PE and PVAc.

In the 1000–1300 cm^{-1} range, the FTIR spectrum shows numerous peaks associated with C-O and C-C vibrations in the PVAc polymer chain. The presence of these bands further confirms that poly(vinyl acetate) is a component of the Zetamix H13 filament. Specific peaks around 1239 cm$^{\wedge-1}$ and 1093 cm^{-1} can be attributed to C-O stretching vibrations, which is consistent with the structure of PVAc [26].

Debinding mechanism of Zetamix filament

The development of FTIR spectra obtained for Zetmix H13 samples at 25 °C (reference sample), after thermal debinding at 350 °C and after thermal debinding at 480 °C, allows the analysis of the thermal debinding process of this felt. The spectrum is in Figure no. 10. Assuming that the main components of this material are polyethylene and polyvinyl acetate, significant changes in the chemical structure after heating can be observed.

The FTIR spectrum of the reference sample (black line) shows characteristic bands for polyethylene and polyvinyl acetate. Peaks in the region of 2916 cm^{-1} and 2848 cm^{-1} correspond to symmetric and asymmetric stretching of the CH$_2$ bonds in polyethylene. In addition, the presence

of bands around 1735 cm^{-1} suggests the presence of ester groups from polyvinyl acetate [26].

After thermal debinding at 350 °C (dashed line), we observe the disappearance of polyethylene-specific bands and ester groups. This suggests that both polymers are degraded at this temperature, leading to the loss of functional groups and the breakdown of the polymer chains.

Upon further heating to 480 °C (dotted line), the band intensities for both polymers are further reduced. The FTIR spectrum indicates almost complete debinding of polyethylene and polyvinyl acetate, which is consistent with the advanced thermal decomposition of these polymers. At this temperature, mainly volatile debinding products are formed, resulting in minimal residual absorption over the entire measured range.

CONCLUSIONS

The conducted thermal analysis of the thermal degradation process enabled the precise determination of the optimal conditions for removing the polymer binder. Based on this analysis, two thermal degradation processes were designed – one for the experimental material and another for the commercial material. The results of the thermogravimetric analysis (TG) and derivative thermogravimetric (DTG) allowed researchers to identify key moments where the most intense degradation of the polymers present in both materials occurs. The maximum degradation rates for the experimental material were observed at 420 °C and 472 °C, while for the

commercial material, they were at 355 °C and 470 °C. This knowledge is significant not only for improving the efficiency of the binder removal process but also for minimizing the risk of material defects, which directly impacts the quality of the final products.

In the second step of the research, the authors demonstrated that the implementation of the solvent degradation stage allowed for a reduction in the irreversible consumption of the binder and enabled the recycling of both the solvent and the ABS polymer. They successfully designed a material and a processing method that does not deviate in quality from commercial materials. Furthermore, the application of solvent degradation allows for the recovery of part of the material for reprocessing, thus fulfilling the principles of sustainable development.

Additionally, the research detailed the qualitative composition of the commercial material, which is crucial for understanding its properties and potential applications. The FTIR analysis revealed that the main components of the Zetamix filament binder are polyethylene and polyvinyl acetate.

The rationale for using experimental filaments in studies of the debinding and sintering processes stems from several key aspects that make them competitive compared to commercial filaments such as Zetamix H13. The commercial filament, developed by NaNo, is characterized by high quality and optimized technological parameters, including a carefully tailored composition and precise processing conditions. Despite this, the experimental filament used in our research does not significantly differ from the commercial product, justifying its use in the context of scientific and industrial analyses.

The advantages of experimental filaments over Zetamix H13 include the ability to adjust the composition parameters, which can offer benefits in specific applications, such as the infiltration of open pore structures in H13 steel sinters. Although the experimental filament has a slightly lower metallic powder loading compared to the commercial filament, key parameters such as particle size distribution remain comparable to those of the commercial counterpart. A significant advantage of the experimental filament is the ability to precisely control the chemical degradation processes, which effectively mitigates differences in polymer content and potential technological issues, such as the formation of surface irregularities on the filament. The disadvantages of

experimental filaments may include greater variability in properties and a lack of full optimization in the manufacturing process, which could affect the quality of final products compared to the refined commercial product, such as Zetamix H13. The higher powder loading in the commercial filament provides it with an advantage in terms of lower polymer content, contributing to better mechanical and surface properties during the sintering process.

In conclusion, despite certain differences, the experimental filament offers promising prospects in studies of sintering and infiltration technologies for H13 steel, especially where the ability to modify composition and process parameters gives it an advantage over commercial filaments.

Acknowledgements

REFERENCES

1. Kadir A. Z. A., Yusof Y., Wahab M. S. Additive manufacturing cost estimation models—a classification review. The International Journal of Advanced Manufacturing Technology 2020, 107, 4033–4053. https://doi.org/10.1007/s00170-020-05262-5

2. Gorjan L., Galusca C., Sami M. Effect of stearic acid on rheological properties and printability of ethylene vinyl acetate based feedstocks for fused filament fabrication of alumina. Additive Manufacturing 2020, 36, 1–25. https://doi.org/10.1016/j.addma.2020.101391

3. Singh G., Missiaen J.M., Bouvard D. Copper extrusion 3D printing using metal injection moulding feedstock: Analysis of process parameters for green density and surface roughness optimization. Additive Manufacturing 2021, 38, 1–40. https://doi.org/10.1016/j.addma.2020.101778

4. Zubrzycki J., Estrada Q., Staniszewski M., Marchewka M. Influence of 3D printing parameters by FDM method on the mechanical properties of manufactured parts. Adv. Sci. Technol. Res. J. 2022, 16, 5, 52–63. https://doi.org/10.12913/22998624/154024

5. Szczęch M., Sikora W. The influence of printing parameters on leakage and strength of fused deposition modelling 3D printed parts. Adv. Sci.

Technol. Res. J. 2024, 18, 1, 195–201. https://doi.org/10.12913/22998624/178330

6. Abdulridha H. H., Abbas T. F., Bedan A. S. Investigate the effect of chemical post processing on the surface roughness of fused deposition modeling printed parts. Adv. Sci. Technol. Res. J. 2024, 18, 2, 47–60. https://doi.org/10.12913/22998624/183528

7. Gocki M., Nowak J. A. Autocatalytic metallization of polymer materials produced by the additive technology, Adv. Sci. Technol. Res. J. 2024, 18, 4, 97–110. https://doi.org/10.12913/22998624/188540

8. Bazarbay B. B., Kurbanova B. A., Absadykov B. N. et. al. Investigation of the effect of thermal post-treatment od density and hardness of a green part printed with FFF technology. Journal of Chemical Technology and Metallurgy 2022, 57, 6, 1258–1266.

9. Thompson Y., Gonzalez-Gutierrez J., Kukla C., et. al. Fused filament fabrication, Debinding and sintering as a low cost additive manufacturing method of 316L stainless steel. Additive Manufacturing 2019, 30. https://doi.org/10.1016/j.addma.2019.100861

10. Ray S., Cooney R.P., Thermal Degradation of polymer and polymer composites. Handbook of Environmental Degradation of Materials. Kutz M, editor. William Andrew Publishing 2018, 17, 185–206. https://doi.org/10.1016/B978-0-323-52472-8.00009-5

11. Pielichowski K., Njuguna J., Majka T. Thermal degradation of polymeric materials, Elsevier 2022. https://doi.org/10.1016/C2019-0-04932-1

12. Singh B., Sharma N. Mechanistic implications of plastic degradation. Polymer Degradation and Stability 2008, 93, 561–584. https://doi.org/10.1016/j.polymdegradstab.2007.11.008

13. Van Krevelen DW. Properties of Polymers. Amsterdam. Elsevier 2009, 16.

14. Mark J. Physical Properties of Polymers Handbook. Springer.

15. Lis J., Pampuch R. Sintering, Book, AGH – Uczelniane Wydawnictwa Naukowo-Dydaktyczne Kraków 2000. (in Polish).

16. Ursi F. Characterization of Metal FDM process and final mechanical performances evaluation, Politecnico di Torino. Department of Mechanical and Aerospace Engineering. Master Thesis. 2023.

17. Chaudhary R., Ali P., Gandhare N., et al. Thermal decomposition kinetics of some transition metal coordination polymers of fumaroyl bis (paramethoxyphenylcarbamide) using DTG/DTA techniques.

Arabian Journal of Chemistry 2019, 12, 1070–1082. https://doi.org/10.1016/j.arabjc.2016.03.008

18. Ramazani H., Kami A. Metal FDM, a new extrusion-based additive manufacturing technology for manufacturing of metallic parts: a review. Progress in Additive Manufacturing 2022, 7, 609–626. https://doi.org/10.1007/s40964-021-00250-x

19. H13 steel Zetamix Filament. https://zetamix.fr/en/produit/filament-zetamix-h13-en/. Accessed 15 Nov 2023.

20. Zetamix General guidelines Tool steel H13. https://zetamix.fr/wp-content/uploads/2023/07/Guideline-H13.pdf. Accessed 15 Nov 2023.

21. Zetamix H13 steel datasheet. https://zetamix.fr/wp-content/uploads/2023/08/Datasheet-Zetamix-H13.pdf. Accessed 15 Nov 2023.

22. Riva L., Fiorentino A., Ceretti E. Characterization of the chemical finishing process with a cold acetone bath of ABS parts fabricated by FFF. Selected Topics in Manufacturing. Lecture Notes in Mechanical Engineering. 2022, 38, 77–89. https://doi.org/10.1007/978-3-030-82627-7_5

23. Arostegui A., Sarrionandia M., Aurrekoetxea J., et al. Effect of dissolution-based recycling on the degradation and the mechanical properties of acrylonitrile–butadiene–styrene copolymer. Polymer Degradation and Stability 2006, 91, 2768–2774. https://doi.org/10.1016/j.polymdegradstab.2006.03.019

24. https://medium.com/@solventwashertx/acetone-recycling-unlocking-cost-savings-and-sustainability-40f1dc30610e. Accessed 15 Nov 2023.

25. Mohamed M.A., Jaafar J., Ismail A.F., et al. Fourier Transform Infrared (FTIR) Spectroscopy, Editor(s): Hilal N, Ismail A, Matsuura T, Membrane Characterization. Elsevier 2017, 3–29.

26. Spinella L., Bosco N. FTIR Investigation of EVA Chemical Bonding Environment and Its Impact on Debond Energy. IEEE Journal of Photovoltaics 2019, 9, 790–795. https://doi.org/10.1109/JPHOTOV.2019.2904219

27. Liu G., Liao Y., Ma X. Thermal behavior of vehicle plastic blends contained acrylonitrile-butadiene-styrene (ABS) in pyrolysis using TG-FTIR. Waste Management 2017, 61, 315–326. https://doi.org/10.1016/j.wasman.2017.01.034

28. Agirre A., Aguirre M., Leiza JR. Characterization of grafting properties of ABS latexes: ATR-FTIR vs NMR spectroscopy. Polymer 2022, 253. https://doi.org/10.1016/j.polymer.2022.124997